AIAA JOURNAL
Vol. 50, No. 9, September 2012

Stabilization of High-Speed Boundary Layer Using Porous Coatings of Various Thicknesses

S. V. Lukashevich,* A. A. Maslov,† and A. N. Shiplyuk‡
Russian Academy of Sciences, 630090, Novosibirsk, Russia
and
A. V. Fedorov§ and V. G. Soudakov¶
Moscow Institute of Physics and Technology, 140180, Zhukovsky, Russia

DOI: 10.2514/1.J051377

Ultrasonically absorptive coatings can suppress the second-mode instability in a hypersonic boundary layer, and thereby delay laminar-turbulent transition. Theory and numerical simulations indicate that this stabilization effect essentially depends on the ultrasonically absorptive coating thickness. It is expected that optimal coatings may be several times thinner than was assumed before. To validate these findings, the ultrasonically absorptive coating thickness effect is investigated on a sharp cone in the Mach 6 wind tunnel. The coatings comprise several layers of a stainless steel wire mesh that mimics textile materials frequently used for thermal protection. The wall-pressure disturbances are measured upstream and downstream of the coated region. It is shown that the coatings stabilize the second mode and its higher harmonics in accordance with the ultrasonically absorptive coating laminarization concept. The experimental growth rates are compared with predictions of the linear stability theory and direct numerical simulations of two-dimensional disturbances. It is found that an optimal coating is approximately five times thinner than ultrasonically absorptive coatings tested in previous experiments. This may facilitate the manufacturing and integration of ultrasonically absorptive coatings into actual thermal protection systems.

Nomenclature

A	=	porous-layer admittance
d	=	wire diameter
f	=	frequency
h	=	pore depth or thickness of porous coating
M	=	Mach number
p	=	pressure disturbance amplitude or pitch of the wire mesh
Re_1	=	unit Reynolds number
S	=	open screen area; w^2/p^2
T	=	mean flow temperature
u, v	=	components of velocity
w	=	aperture width of the wire mesh
x, y	=	Cartesian coordinates
α	=	wave number
μ	=	viscosity coefficient
ϕ	=	porosity
ω	=	circular frequency

Subscripts

e	=	upper boundary-layer edge
w	=	wall
∞	=	freestream
0	=	stagnation point quantities
1	=	upstream station of the pressure sensor
2	=	downstream station of the pressure sensor

Superscript

$*$	=	dimensional quantities

Presented at the 40th Fluid Dynamics Conference and Exhibit, Chicago, IL, 28 June–1 July 2010; received 25 May 2011; revision received 26 October 2011; accepted for publication 27 December 2011.

*Junior Research Scientist, Khristianovich Institute of Theoretical and Applied Mechanics, Siberian Branch; lukashevich@itam.nsc.ru.

†Deputy Director, Khristianovich Institute of Theoretical and Applied Mechanics, Siberian Branch; Professor, Novosibirsk University; maslov@itam.nsc.ru. Member AIAA.

‡Deputy Director, Khristianovich Institute of Theoretical and Applied Mechanics, Siberian Branch; shiplyuk@itam.nsc.ru.

§Associate Professor, Department of Aeromechanics and Flight Engineering; fedorov@falt.ru. Senior Member AIAA.

¶Associate Professor, Department of Aeromechanics and Flight Engineering; vit_soudakov@mail.ru. Member AIAA.

I. Introduction

LAMINAR-TURBULENT transition causes significant increase in heat transfer and viscous drag that leads to severe restrictions on the performance of high-speed vehicles [1]. This motivates the development of hypersonic laminar flow control (LFC) concepts to delay the transition onset [2]. Under hard environmental conditions of hypersonic flight (high temperatures and large heat fluxes to aerodynamic surfaces), passive LFC methods are of primary interest. Apparently, the first step in this direction is the shaping of aerodynamic bodies, e.g., predominantly the two-dimensional (2-D) shape of the X-43A vehicle was developed to minimize the crossflow instability [3]. For this wedgelike configuration with an aerodynamically smooth surface, dominant instabilities on the upper surface are the first and/or second modes. Because the first mode is stabilized by natural cooling, transition can be triggered by the second-mode instability.

Fedorov et al. [4] showed theoretically that an ultrasonically absorptive coating (UAC), which is a thin porous layer with a fine microstructure, can strongly stabilize the second mode and, presumably, increase the laminar run. These predictions were made using the linear stability theory (LST). Further experimental and theoretical studies [5–13] confirmed this LFC concept. It has been shown that porous coatings of random and regular microstructures can massively suppress the second mode and significantly (more than twice) increase the laminar run in high-speed boundary-layer flows on sharp cones at zero angle of attack.

Two-dimensional direct numerical simulations (DNSs) [14] of the near-wall flow on a flat plate, sharp cone, and compression corner showed that flow nonuniformities, associated with the boundary-layer growth and junctures between coated and uncoated regions,

weakly affect the UAC integral performance. For the compression corner flow, the porous coating strongly stabilizes the second mode in the reattached boundary layer downstream of the separation bubble.

To get an insight into microscale processes inside the porous coating, Brès et al. [15] have conducted 2-D DNS of the interaction of incident acoustic waves with an array of equally spaced micro-cavities on a flat plate surface without flow. It was shown that the reflection coefficients predicted by DNS agree well with the theoretical modeling. The numerical simulations also highlighted the presence of resonant acoustic modes caused by the coupling of small-scale scattered waves near the UAC surface. The cavity depth and the porosity were identified as the most important parameters for UAC design. Guidelines for the choice of these parameters were suggested.

Numerical simulations [16,17] of disturbances in the temporally evolving boundary layer were conducted for relatively deep pores operating in attenuation regimes as well as for shallow pores operating in cancellation/reinforcement regimes with alternating regions of local minima and maxima of the coating acoustic absorption. These simulations confirmed the results of LST that employs impedance boundary conditions.

Sandham and Lüdeke [18] conducted DNS of the temporal stability for the boundary-layer flow over UAC comprising equally spaced 2-D cavities and three-dimensional (3-D) pores of rectangular cross section. Fedorov [19] compared these numerical solutions with the theory and showed that the theoretical model holds in much wider range of the UAC thickness and pore sizes than it was expected before. Similar comparisons have been made by Wartemann et al. [20].

The aforementioned DNS studies suggest a relaxation of the original restrictions on the UAC parameters and seek optimal porous coatings in a wider parameter space. Namely, it is feasible to optimize the UAC performance with respect to the porous layer thickness. The theory [4] and DNS [17,20] show that, for disturbance of particular frequency, there is an optimal UAC thickness at which the reflection of the disturbance from the pore bottom leads to the phase cancellation and maximum stabilization of the second-mode waves. With further increasing of the UAC thickness, the stabilization effect slightly decreases and ultimately tends to a constant level corresponding to the deep pore limit. These predictions need to be verified experimentally. Herein, the UAC thickness effect is investigated on a sharp cone in the hypersonic tunnel TRANZIT-M of the Khristianovich Institute of Theoretical and Applied Mechanics (ITAM), Siberian Branch of the Russian Academy of Sciences, at the freestream Mach 6. The experimental results are compared with predictions of LST and DNS.

II. Experimental Setup

Experiments were carried out in the ITAM hypersonic tunnel TRANZIT-M at the freestream Mach number $M_\infty = 6$ and the unit Reynolds number $Re_{1\infty} = 4.5 \times 10^6$ m^{-1}. The wind-tunnel layout appears in Fig. 1; shown are the electric heater (1), fast-acting valve (2), plenum chamber (3), settling chamber (4), frame (5), nozzle (6), test section (7), optical windows (8), isolated pedestal for model installation (9), diffuser (10), and vacuum tank (11). Air was heated up by ohmic heaters and gathered in the plenum chamber under pressure up to 200 bar. After opening the fast-acting valve, air flowed to the settling chamber and to the test section through the contoured nozzle of 300 mm exit diameter. Then, gas was compressed by a diffuser and flowed to the vacuum tank. The run time was about 110–200 ms.

Unfortunately, there are no data on the freestream noise in this tunnel at $M_\infty = 6$. Measurements of the $p_0^{*\prime}$ pressure pulsations (behind a normal shock) have been conducted in the frequency band from 1 to 200 kHz at $M_\infty = 4$. The rms value of these pulsations is $4.0 \pm 0.2\%$ at the stagnation pressures 4 and 8 bar, and the stagnation temperatures 290 and 450 K. Although the TRANZIT-M wind tunnel is a conventional noisy facility, the freestream noise is relatively small in the high-frequency band related to the second-mode instability and its higher harmonics. This allowed the authors to identify the second-mode waves in the boundary layer on the cone model and to measure their stability characteristics.

The model is a 7 deg half-angle sharp cone of 0.42 m length (Fig. 2) that was tested at nominally zero angle of attack. The UAC strip was flash mounted on the solid backup between the streamwise stations (measured from the cone tip along the cone surface) 361.3 and 386.3 mm (the strip width is $\Delta x^* = 25$ mm).

The coatings comprise several layers of the stainless steel wire mesh (Haver & Boecker) schematically shown in Fig. 3a. The mesh parameters are the aperture width ($w^* = 0.1$ mm), the wire diameter ($d^* = 0.025$ mm), and the open screen area (64%). The thickness of one layer is approximately 0.04 mm. Each layer was oriented with respect to the previous one at the 45 deg angle. Experiments were conducted with the six coatings listed in Table 1. The magnified top view of coating 6 having 10 mesh layers is shown in Fig. 3b.

To evaluate the stability characteristics of the boundary-layer flow, the wall-pressure disturbances were measured at the stations $x_1^* = 352.7$ mm and $x_2^* = 394.9$ mm located just upstream and downstream of the coating boundaries (Fig. 2). The measurements were carried out using the high-frequency piezoelectric pressure gauges PCB132A31, which have a diameter of 3 mm and frequency band from 11 kHz to 1 MHz.

III. Experimental Results

The wind-tunnel runs were performed at the stagnation temperature $T_0^* = 353$ K and the total pressure $p_0^* = 0.33$ MPa. The model has the wall temperature $T_w^* = 290$ K. The flow parameters at the upper boundary-layer edge (which are assumed to be constant for a sharp cone at zero angle of attack) are $M_e = 5.35$, $T_e^* = 52.5$ K, and $Re_{e1} = 5.7 \times 10^6$ m^{-1}. These parameters are determined by solving the Navier–Stokes equations for perfect gas with constant specific heat ratio of $\gamma = 1.4$ and Pr =0.72.

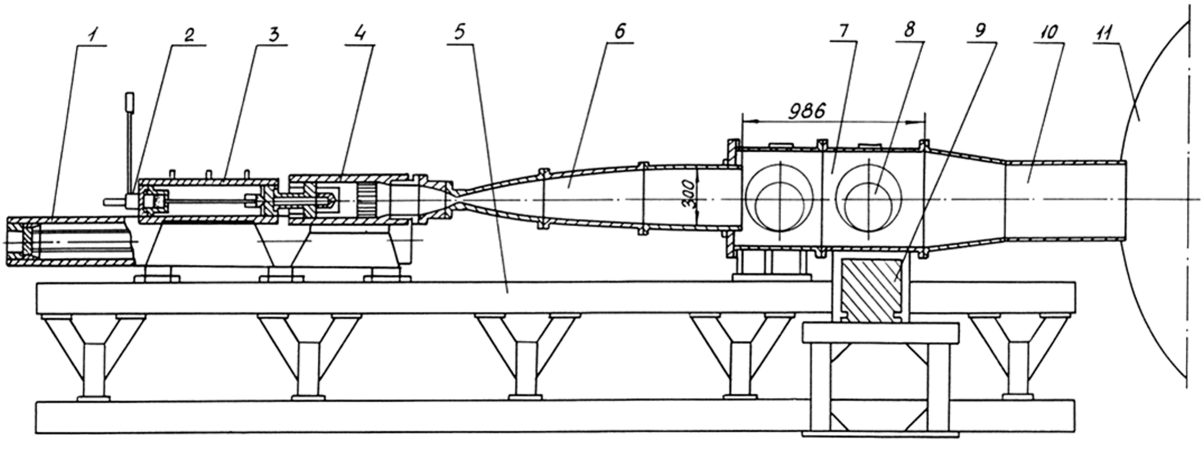

Fig. 1 Layout of TRANZIT-M wind tunnel; dimensions are given in millimeters.

Table 1 Coatings

Coating number	Number of layers	Total thickness, mm
1	1	0.04
2	2	0.07
3	4	0.15
4	6	0.24
5	8	0.34
6	10	0.39

Figure 4a shows the pressure disturbance spectra $p_1^*(f^*)$ measured at the front station x_1^* on the cone with different coatings. The first peak (in the frequency band from 100 to 220 kHz) corresponds to the second-mode wave packet. The presence of a second harmonic induced by this wave packet indicates that nonlinear effects are appreciable in the considered x stations. A good insight into the effect of porous surface on the nonlinear breakdown is given by the experiment of Chokani et al. [21] and DNSs of De Tullio and Sandham [22]. As expected, the upstream pressure gauge was not affected by the coating; all spectra are almost identical in the frequency band 50–400 kHz. This allowed the authors to use the same $p_1^*(f^*)$ for analysis of all the cases. Hereafter, the distribution $p_1^*(f^*)$ corresponds to the spectrum measured on the cone with solid surface.

The disturbance spectra $p_2^*(f^*)$ measured in the station x_2^* (behind the coatings) are shown in Fig. 4b. As the UAC thickness increases, the second-mode peak decreases and its maximum is shifted to lower frequencies. The high-frequency peak is also suppressed. For coatings 4, 5, and 6 having $h^* \geq 0.24$ mm, the spectrum no longer depends on the coating thickness. Thus, the coatings stabilize the second mode and its higher harmonics in accordance with the UAC LFC concept [4]. The low-frequency disturbances are marginally destabilized, which is consistent with the experimental observations [6] on the felt-metal coating of random microstructure. On the regular UAC, which has a smoother surface, this detrimental effect is essentially weaker [11]. The growth of low-frequency disturbances could be caused by distributed roughness of UAC and/or by destabilization of the oblique first mode. This issue remains to be clarified.

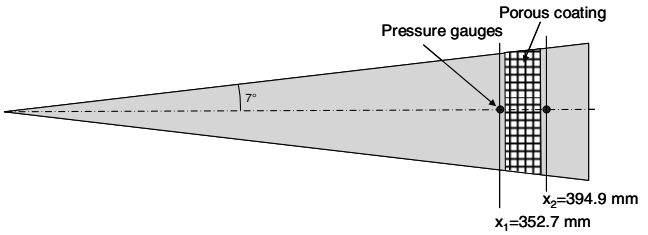

Fig. 2 Schematics of the sharp cone model with the porous coating and pressure gauges.

To evaluate the UAC stabilization effect, the growth rates of the spectral components are calculated using the relation

$$-\alpha_i = \frac{\ell_n(p_2^*/p_1^*)}{2(R_2 - R_1)} \tag{1}$$

in which $R_{1,2} = \sqrt{U_e^* x_{1,2}^*/\nu_e^*}$ is the local Reynolds number based on the flow parameters at the upper boundary-layer edge and Blasius's length scale $\Delta^* = \sqrt{\nu_e^* x^*/U_e^*}$ (U_e^* and ν_e^* are velocity and kinematic viscosity, respectively). Figure 5 shows the growth rates for disturbances of typical frequencies as functions of the UAC thickness h^*. Maximal stabilization of the second-mode waves is observed at $h^* \approx 0.15$ mm (coating 3 having four mesh layers). With further increase of h^*, the UAC performance slightly decreases and achieves a constant level starting from $h^* \approx 0.25$ mm. This trend is consistent with the theoretical dependencies reported in [4] and DNS studies [20]. Note that a very thin coating may slightly destabilize the disturbance (e.g., see the line for $f^* = 125$ kHz). A similar effect was predicted by theory and numerical simulations [19].

IV. Theoretical Model and DNS

A. Linear Stability Problem

In the framework of the theoretical model developed in [4,6,8], the linear stability problem is solved for the boundary-layer flow having

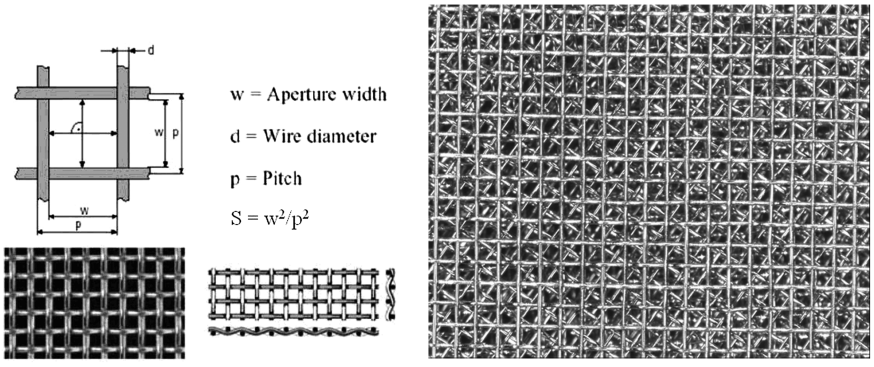

a) b)

Fig. 3 a) Schematic view of the wire mesh and b) magnified view of coating 6 comprising 10 mesh layers.

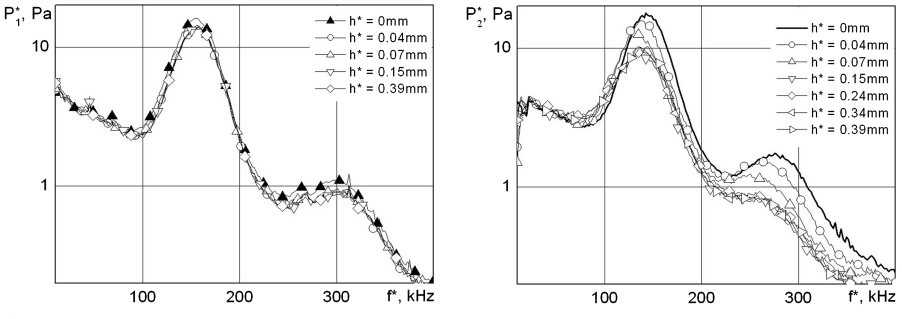

a) b)

Fig. 4 Wall-pressure disturbance spectra measured in the a) front station $x_1^* = 352.7$ mm and in the b) rear station $x_2^* = 394.9$ mm.

the upper-edge parameters specified in Sec. III. The gas is perfect with a Prandtl number of 0.72 and a specific heat ratio of $\gamma = 1.4$. The mean flow is calculated using self-similar solutions of the boundary-layer equations at zero pressure gradient (compressible Blasius's solutions with the Mangler transformation from the planar to axisymmetric configuration). Preliminary computations showed that these solutions agree well with the Navier–Stokes solutions for the axisymmetric flow in the x stations considered hereafter. It is assumed that the mean flows on both porous and solid surfaces are identical. The dynamic viscosity μ is calculated using the Sutherland formula with a constant temperature of 110.4 K, and the second viscosity is assumed to be zero. The spatial stability problem is solved for 2-D disturbances of the traveling waveform having the real circular frequency ω and the complex eigenvalue $\alpha = \alpha_r + i\alpha_i$, in which $-\alpha_i$ represents the spatial growth rate. For the local-parallel mean flow, the ordinary differential equation (ODE) system of stability equations is integrated with the following boundary conditions on the porous wall:

$$u(0) = 0, \qquad v(0) = Ap'(0), \qquad \theta(0) = 0 \tag{2}$$

in which $u(y)$, $v(y)$, $p'(y)$, and $\theta(y)$ are amplitude functions of disturbances of the velocity components, pressure, and temperature, respectively. The porous-layer admittance A is expressed as [4]

$$A = -\frac{\phi}{Z_0}\tanh(mH) \tag{3}$$

Here, $H = h^*/\Delta^*$ is the nondimensional thickness of the porous layer, and ϕ is porosity. The characteristic impedance Z_0 and the propagation constant m are calculated using the analytical solutions [8] obtained for the coating comprising equally spaced cylindrical pores of square cross section, with the square side being equal to the aperture width w^*(see Fig. 3). The UAC porosity, calculated as the ratio of empty volume to the total volume, is $\phi = 0.8$. The slip effect associated with Knudsen layers on the mesh wires is neglected. Note that this theoretical model does not capture all details of the actual structure shown in Fig. 3b. It should be treated as a first-cut approximation of rather complicated physics related to the interaction of acoustic disturbances with the cylindrical elements (wires), e.g., the porous layer admittance may be affected by the presence of diagonal elements and openings between the neighboring meshes. The given computational results provide only a means for prediction of basic trends associated with the coating thickness.

It should also be noted that the local stability problem does not capture the coating end effects related to the upstream and downstream boundaries of the coated region. In accord with Eq. (1), the LST computations have been carried out for the midstation $x_0^* = (x_1^* + x_2^*)/2 = 301.3$ mm.

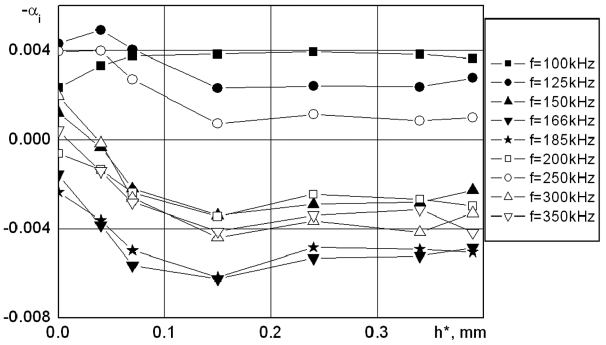

Fig. 5 Growth-rate distributions $-\alpha_i(h^*)$ for disturbances of different frequencies f^*.

Table 2 Frequencies

f^*, kHz	ω
60	198.3
90	297.4
100	330.4
110	363.5
120	396.5
130	429.5
160	528.7

B. DNS Setup

The Navier–Stokes equations for unsteady axisymmetric flow are solved numerically. The numerical setup is similar to that reported in [14]. The nondimensional coordinates, time, and flow parameters are

$$(x, y) = (x^*, y^*)/L^*, \qquad t = t^* U_\infty^*/L^*$$
$$(u, v) = (u^*, v^*)/U_\infty^*, \qquad p = p^*/(\rho_\infty^* U_\infty^{*2})$$

in which $L^* = 0.415$ m is the cone length measured along its surface, and U_∞^* is the freestream velocity. For the solid-wall case, no-slip boundary conditions $(u, v) = 0$ are imposed on the cone surface. The wall temperature is fixed, and the temperature disturbance on the wall surface is zero.

The boundary conditions on the UAC surface are formulated using an analytical relation [Eqs. (2) and (3)], which couples the wall-normal velocity disturbance with the pressure disturbance. In terms of real variables, this relation is written as

$$v_{w,n}(x, t) = p'_w(x, t)\mathrm{Real}(A) - \frac{1}{\omega}\frac{\partial}{\partial t}(p'_w(x, t))\mathrm{Imag}(A) \tag{4}$$

in which $p'_w(x, t) = p_w(x, t) - p_w(x, 0)$ is pressure disturbance on the wall surface (difference between instant and steady-state pressure), and $\omega = 2\pi f^* L^*/U_\infty^*$ is dimensionless secular frequency. In Eq. (4), the time derivative is approximated with the second-order accuracy. The UAC admittance A is calculated using Eq. (3) with the appropriate nondimensionalization. The boundary condition [Eq. (4)] is applied to the coated region $0.87 < x < 0.93$.

Note that the impedance boundary condition [Eq. (4)] is obtained by averaging the disturbance field over the surface region containing large number of pores, i.e., it is assumed that the boundary-layer disturbance wavelength is much larger than the pore spacing. This approximation does not account for small-scale processes near the pore mouths. The DNS does not resolve flowfields inside cavities and near their openings. Nevertheless, nonparallel effects and the coating boundary effects, which have the length scale approximately equal to the boundary-layer thickness, are simulated correctly.

The computational domain is a rectangle with its bottom side corresponding to the cone surface. On the outflow boundary, the

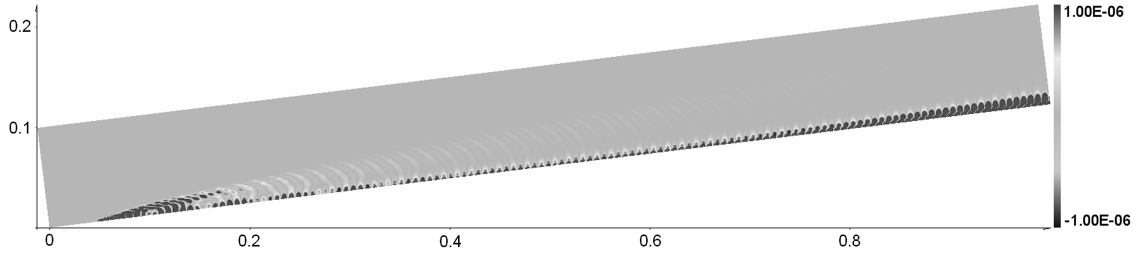

Fig. 6 Pressure disturbance field at frequency $f^* = 120$ kHz ($\omega = 396.5$).

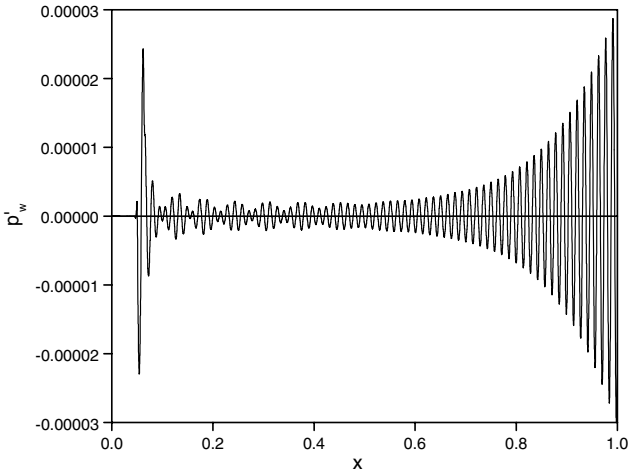

Fig. 7 Wall-pressure disturbance at frequency $f^* = 120$ kHz ($\omega = 396.5$).

variables are extrapolated using the linear approximation to minimize upstream effects of this boundary on the disturbance field. On the inflow and upper boundaries, the boundary conditions correspond to the freestream (Dirichlet boundary conditions). The upper boundary is located above the cone-induced shock wave.

The problem is solved in two steps. First, the steady-state solution is calculated to provide the mean flowfield. Second, unsteady disturbances are introduced by the boundary condition providing local periodic suction blowing near the cone nose. The suction-blowing mass flow is specified as

$$q_w(x,t) = \frac{\rho_w^* v_w^*}{\rho_\infty^* U_\infty^*} = \varepsilon \sin\left(2\pi \frac{x - x_{S1}}{x_{S2} - x_{S1}}\right) \sin(\omega t), \quad x_{S1} \le x \le x_{S2}, \qquad t > 0 \tag{5}$$

in which the amplitude, $\varepsilon = 1 \times 10^{-4}$, is chosen small enough to compare numerical results with the LST; $x_{S1} = 0.05$ and $x_{S2} = 0.064$ are boundaries of the suction-blowing region.

The problem is solved numerically using the implicit second-order finite-volume method described in [23]. The Navier–Stokes equations for axisymmetric flow are approximated by a conservative shock-capturing scheme. The advection terms are approximated by the third-order weighted essentially nonoscillatory scheme. Although this computational scheme is dissipative, its numerical dissipation can be suppressed using a sufficiently fine computational grid. Herein, the computational grid has 3001×251 nodes with clustering of the grid nodes in the boundary-layer region. There are at least 45 grid nodes per the disturbance wavelength. As shown in [23,24], the foregoing grid resolution is appropriate for simulations of the boundary-layer stability and receptivity. The governing equations, the code algorithm, implementation, and validations can be found in [23].

V. DNS Results

For the solid-wall case, computations have been carried out at the actuator frequencies given in Table 2. The porous-wall cases have

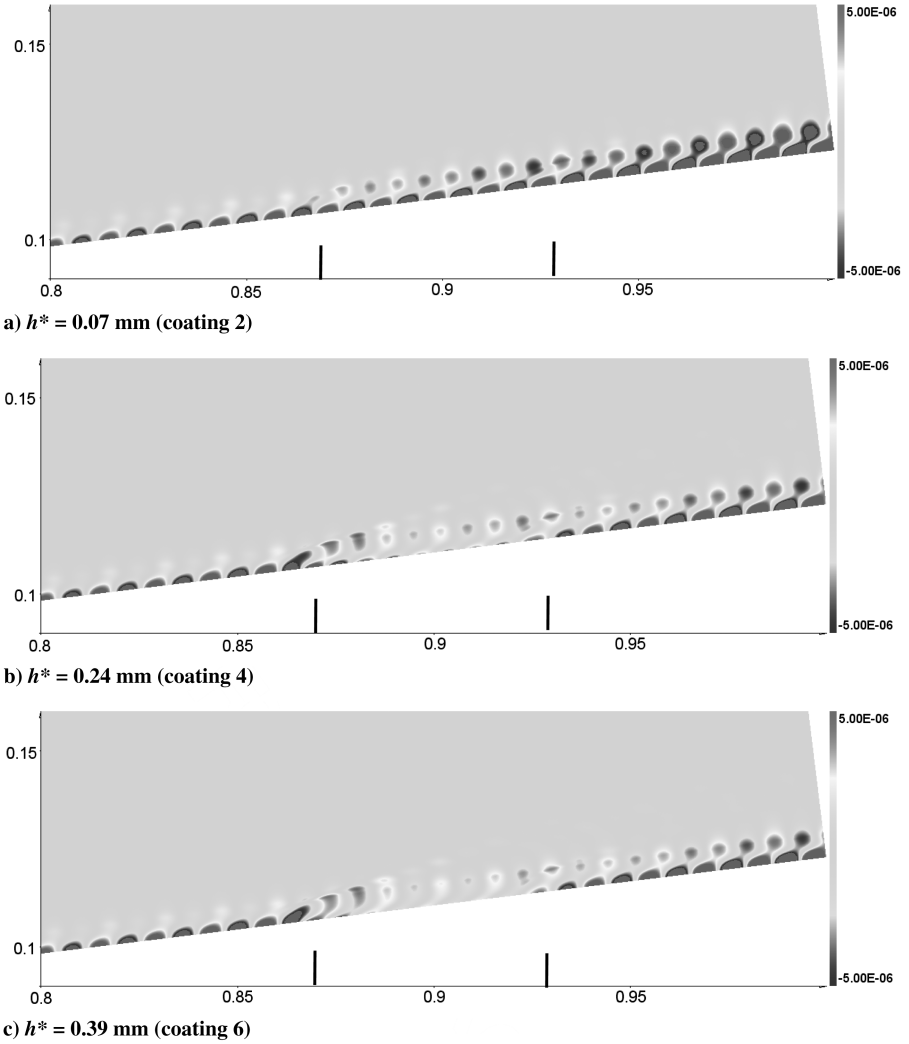

a) $h^* = 0.07$ mm (coating 2)

b) $h^* = 0.24$ mm (coating 4)

c) $h^* = 0.39$ mm (coating 6)

Fig. 8 Pressure disturbance fields at $f^* = 120$ kHz; the coated region is $0.87 < x < 0.93$.

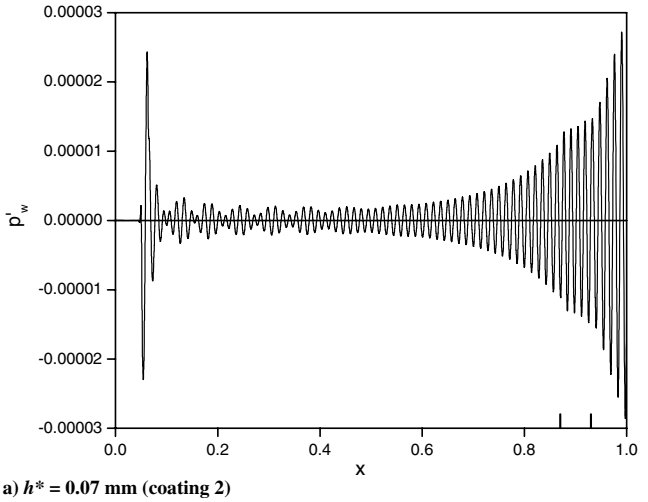

a) $h^* = 0.07$ mm (coating 2)

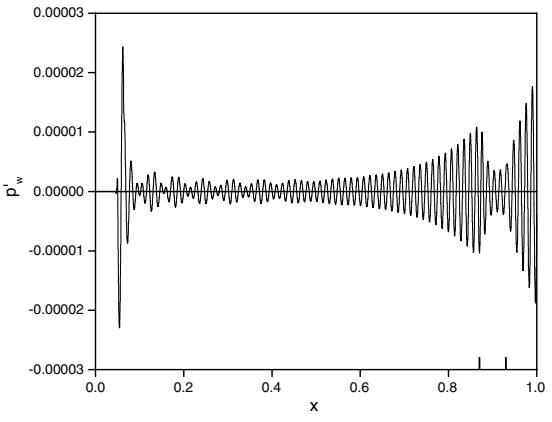

b) $h^* = 0.24$ mm (coating 4)

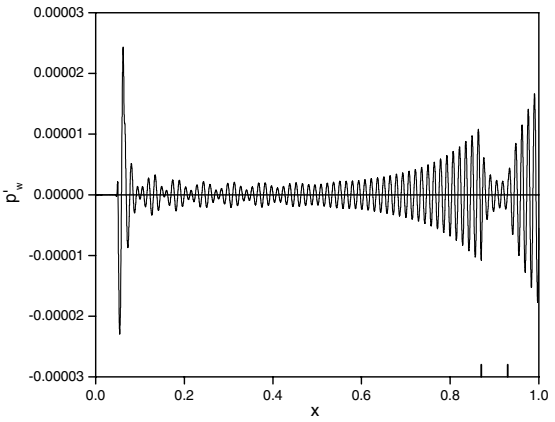

c) $h^* = 0.39$ mm (coating 6)

Fig. 9 Distributions of the wall-pressure disturbance, $f^* = 120$ kHz; the coated region is $0.87 < x < 0.93$.

been simulated at the frequencies 110 and 120 kHz, which correspond to the unstable frequency band of the second mode.

As an example, Fig. 6 shows the pressure disturbance field at $f^* = 120$ kHz for the solid-wall case. The corresponding distribution of the wall-pressure disturbances is shown in Fig. 7. After the transient process, the disturbance grows exponentially and its spatial structure approaches the second-mode shape function.

Figures 8 and 9 show similar data for the porous-wall cases at $f^* = 120$ kHz. The coated region lies in the range $0.87 < x < 0.93$ (vertical lines in Figs. 8 and 9). For the coatings of relatively small thickness ($h^* < 0.15$ mm), the UAC boundary effects are not pronounced. The disturbance growth drops in the coated region almost instantly without noticeable scattering of the boundary-layer disturbance at the UAC boundaries (Figs. 8a and 9a for $h^* = 0.07$ mm). For thicker coatings, the scattering leads to radiation of acoustic waves by the UAC front boundary (Figs. 8b and 8c). This causes a sudden drop of the disturbance amplitude on the coated surface (Figs. 9b and 9c). The boundary effect increases with the UAC thickness.

VI. Comparisons with Experiment

A. Solid-Wall Case

The first series of computations has been conducted for the solid-wall case. In accord with the experimental data, the DNS growth rates are calculated using Eq. (1), in which the amplitudes $p_1 = p(x_1)$ and $p_2 = p(x_2)$ are determined from the numerical distributions of the wall-pressure disturbances. The LST growth rates are calculated at the midstation $x_0 = (x_1 + x_2)/2$. As shown in Fig. 10, the DNS solutions agree satisfactorily with the experimental data in the second-mode frequency band. The LST predicts well the frequency of maximal instability, while the maximum growth rate is larger and the unstable frequency band is narrower than in the experiment. Note that measurements are carried out for natural disturbances. The comparison indicates that 2-D second-mode waves are dominant in the natural disturbance spectra measured on the cone surface.

B. Porous-Wall Cases

For the porous-wall cases, the DNS growth rates have been calculated using Eq. (1). The LST calculations have been conducted for the UAC midstation. The distributions of $-\alpha_i(h^*)$ for frequencies related to the second-mode instability are shown in Fig. 11. The LST

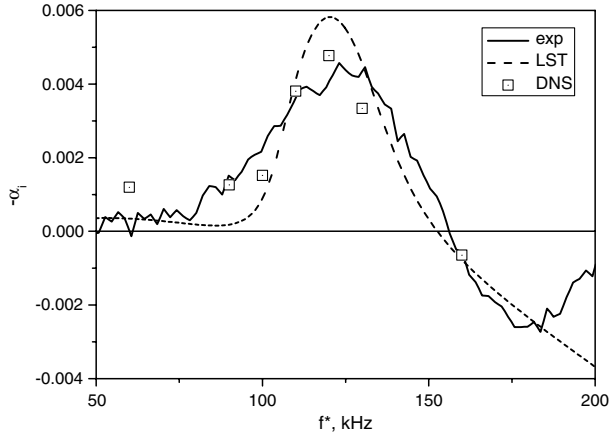

Fig. 10 Growth rates $-\alpha_i$ vs frequency f^* at $x_1^* = 352.7$ mm, the solid-wall case; exp denotes experiment.

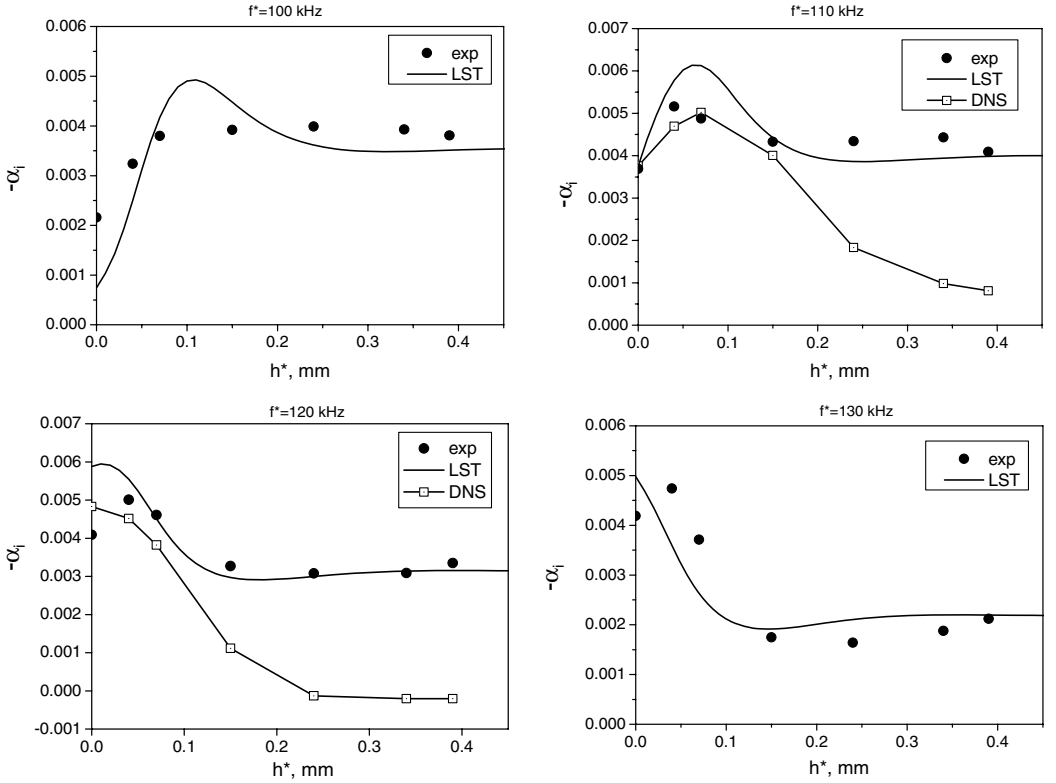

Fig. 11 Growth rate distributions $-\alpha_i(h^*)$ for the second-mode disturbance frequencies; exp denotes experiment.

predictions are remarkably close to the experimental data. The DNS distributions are consistent with the experiment and LST for relatively thin coatings having $h^* \leq 0.15$ mm. This corresponds to the UAC thickness ratio of $h^*/b^* \leq 3$, in which $b^* = w^*/2$ is half-width of the effective pore cross section. For thicker coatings, the DNS predicts essentially stronger stabilization. This overestimate of the UAC performance is associated with the UAC boundary effect observed in the DNS solutions (see Sec. V). A sudden drop of the disturbance amplitude at the UAC front boundary (Figs. 9b and 9c) leads to significant reduction of the amplitude ratio p_2/p_1 and, in accord with Eq. (1), decreasing of $-\alpha_i$. Presumably, this boundary effect is not realized in the experiment. Furthermore, the numerical simulation does not account for the fine structure (microholes, roughness, etc.) that may produce appreciable effects on disturbances near the coating boundaries.

The foregoing results indicate that there is an optimal UAC thickness at which the second-mode stabilization is maximal. For the data shown in Fig. 11 (see plots relevant to frequencies 120 and 130 kHz), the optimum corresponds to the UAC thickness ratio of $h/b \approx 3$. This value correlates well with the parametric studies, which were conducted for the porous coating comprising equally spaced cylindrical pores of circular cross section [13].

VII. Conclusions

The ultrasonically absorptive coating (UAC) thickness effect has been investigated on a 7 deg half-angle sharp cone at zero angle of attack in the Institute of Theoretical and Applied Mechanics hypersonic tunnel TRANZIT-M at the freestream Mach 6. For this purpose, UAC strips of various thicknesses have been installed on the cone surface, and the wall-pressure disturbances have been measured just upstream and downstream of the coated region. The coatings comprise several layers of a stainless steel wire mesh that mimics textile materials frequently used for thermal protection. Fourier analysis of the measured pressure pulsations provides the disturbance spectra in a frequency band covering the second-mode instability and its higher harmonic. These data allowed the authors to evaluate the disturbance growth rates on the solid and porous walls, and to estimate the UAC performance vs the porous-layer thickness.

The experiments showed that the coatings stabilize the second mode and its higher harmonics in accord with the UAC laminarization concept. The low-frequency disturbances are marginally destabilized, which is consistent with the previous experimental observations on the felt-metal coating of random microstructures. Presumably, destabilization of the low-frequency disturbances is associated with distributed roughness. On UAC of regular microstructure having a smoother surface, this detrimental effect is essentially weaker.

Direct numerical simulations (with the impedance boundary condition on the coated surface) showed that, for relatively thick coatings, scattering of the boundary-layer disturbance on the UAC front boundary leads to radiation of acoustic waves. This causes a sudden drop of the disturbance amplitude on the coated region. However, this boundary effect is not confirmed by the experimental data. Detailed measurements of the disturbance field near the coating boundaries are needed to clarify this issue.

It was found that, in accord with the theoretical predictions, there is an optimal UAC thickness at which the second-mode stabilization is maximal. This optimum corresponds to the UAC thickness ratio of $h/b \approx 3$ that is consistent with the theory. A similar optimal ratio has been predicted theoretically for quite different UAC microstructure having equally spaced cylindrical blind pores of circular cross section. These findings allowed the authors to assume that an optimal UAC thickness ratio can be established for sufficiently wide ranges of basic parameters. It is important to note that the optimal coating be approximately five times thinner than those tested in previous experiments. This may facilitate the manufacturing and integration of UAC into actual thermal protection systems.

Acknowledgments

This work is supported by the Russian Foundation for Basic Research (grant numbers 09-08-01117 and 09-08-00557-a) and partially (A. V. Fedorov) by the U.S. Air Force Office of Scientific Research/NASA National Center for Hypersonic Laminar-Turbulent Transition.

References

[1] Schneider, S. P., "Hypersonic Laminar-Turbulent Transition on Circular Cones and Scramjet Forebodies," *Progress in Aerospace Sciences*, Vol. 40, Nos. 1–2, Feb. 2004, pp. 1–50. doi:10.1016/j.paerosci.2003.11.001

[2] Kimmel, R. L., "Aspects of Hypersonic Boundary-Layer Transition Control," AIAA Paper 2003-772, 6–9 Jan. 2003.

[3] Berry, S., Daryabeigi, K., Wurster, K., and Bittner, R., "Boundary Layer Transition on X-43A," AIAA Paper 2008-3736, 23–26 June 2008.

[4] Fedorov, A. V., Malmuth, N. D., Rasheed, A., and Hornung, H. G., "Stabilization of Hypersonic Boundary Layers by Porous Coatings," *AIAA Journal*, Vol. 39, No. 4, April 2001, pp. 605–610. doi:10.2514/2.1382

[5] Rasheed, A., Hornung, H. G., Fedorov, A. V., and Malmuth, N. D., "Experiments on Passive Hypervelocity Boundary Layer Control Using an Ultrasonically Absorptive Surface," *AIAA Journal*, Vol. 40, No. 3, 2002, pp. 481–489. doi:10.2514/2.1671

[6] Fedorov, A., Shiplyuk, A., Maslov, A., Burov, E., and Malmuth, N., "Stabilization of a Hypersonic Boundary Layer Using an Ultrasonically Absorptive Coating," *Journal of Fluid Mechanics*, Vol. 479, 2003, pp. 99–124. doi:10.1017/S0022112002003440

[7] Fedorov, A., Kozlov, V., Shiplyuk, A., Maslov, A., Sidorenko, A., Burov, E., and Malmuth, N., "Stability of Hypersonic Boundary Layer on Porous Wall with Regular Microstructure," AIAA Paper 2003-4147, June 2003.

[8] Kozlov, V. F., Fedorov, A. V., and Malmuth, N. D., "Acoustic Properties of Rarified Gases Inside Pores of Simple Geometries," *Journal of the Acoustical Society of America*, Vol. 117, No. 6, June 2005, pp. 3402–3412. doi:10.1121/1.1893428

[9] Chokani, N., Bountin, D. A., Shiplyuk, A. N., and Maslov, A. A., "Nonlinear Aspects of Hypersonic Boundary Layer Stability on a Porous Surface," *AIAA Journal*, Vol. 43, No. 1, Jan. 2005, pp. 149–155. doi:10.2514/1.9547

[10] Fedorov, A., Shiplyuk, A., Maslov, A., Kozlov, V., Sidorenko, A., and Malmuth, N., "Hypersonic Laminar Flow Control Using a Porous Coating of Random Microstructure," AIAA Paper 2006-1112, 9–12 Jan. 2006.

[11] Fedorov, A. V., Kozlov, V. F., and Addison, R. C., "Reflection of Acoustic Disturbances from a Porous Coating of Regular Microstructure," AIAA Paper 2008-3902, 23–26 June 2008.

[12] Maslov, A. A., Fedorov, A. V., Bountin, D. A., Shiplyuk, A. N., Sidorenko, A. A., and Malmuth, N. D., "Experimental Study of Transition in Hypersonic Boundary Layer on Ultrasonically Absorptive Coating with Random Porosity," AIAA Paper 2008-587, 7–10 Jan. 2008.

[13] Fedorov, A. V., and Malmuth, N. D., "Parametric Studies of Hypersonic Laminar Flow Control Using a Porous Coating of Regular Microstructure," AIAA Paper 2008-588, 7–10 Jan. 2008.

[14] Egorov, I. V., Fedorov, A. V., Novikov, A. V., and Soudakov, V. G., "Direct Numerical Simulation of Supersonic Boundary-Layer Stabilization by Porous Coatings," AIAA Paper 2007-948, 8–11 Jan. 2007.

[15] Brès, G. A., Colonius, T., and Fedorov, A. V., "Acoustic Properties of Porous Coatings for Hypersonic Boundary-Layer Control," *AIAA Journal*, Vol. 48, No. 2, Feb. 2010, pp. 267–274. doi:10.2514/1.40811

[16] Brès, G. A., Colonius, T., and Fedorov, A. V., "Stability of Temporally Evolving Supersonic Boundary Layers over Micro-Cavities for Ultrasonic Absorptive Coatings," AIAA Paper 2008-4337, 23–26 June 2008.

[17] Brès, G. A., Inkman, M., Colonius, T., and Fedorov, A. V., "Alternate Designs of Ultrasonic Absorptive Coatings for Hypersonic Boundary Layer Control," AIAA Paper 2009-4217, 22–25 June 2009.

[18] Sandham, N. D., and Lüdeke, H., "Numerical Study of Mach 6 Boundary-Layer Stabilization by Means of a Porous Surface," *AIAA Journal*, Vol. 47, No. 9, Sept. 2009, pp. 2243–2252. doi:10.2514/1.43388

[19] Fedorov, A. V., "Temporal Stability of Hypersonic Boundary Layer on Porous Wall: Comparison of Theory with DNS," AIAA Paper 2010-1242, 4–7 Jan. 2010.

[20] Wartemann, V., Lüdeke, H., and Sandham, N. D., "Stability Analysis of Hypersonic Boundary Layer Flow over Microporous Surfaces," AIAA Paper 2010-7202, 19–22 Oct. 2009.

[21] Chokani, N., Bountin, D. A., Shiplyuk, A. N., and Maslov, A. A., "Nonlinear Aspects of Hypersonic Boundary-Layer Stability on a Porous Surface," *AIAA Journal*, Vol. 43, No. 1, Jan. 2005, pp. 149–155. doi:10.2514/1.9547

[22] De Tullio, N., and Sandham, N. D., "Direct Numerical Simulation of Breakdown to Turbulence in a Mach 6 Boundary Layer over a Porous Surface," *Physics of Fluids*, Vol. 22, No. 9, 2010, p. 094105. doi:10.1063/1.3481147

[23] Egorov, I. V., Fedorov, A. V., and Soudakov, V. G., "Direct Numerical Simulation of Disturbances Generated by Periodic Suction-Blowing in a Hypersonic Boundary Layer," *Theoretical and Computational Fluid Dynamics*, Vol. 20, No. 1, 2006, pp. 41–54. doi:10.1007/s00162-005-0001-y

[24] Egorov, I. V., Fedorov, A. V., and Soudakov, V. G., "Receptivity of a Hypersonic Boundary Layer over a Flat Plate with a Porous Coating," *Journal of Fluid Mechanics*, Vol. 601, 2008, pp. 165–187.

A. Tumin
Associate Editor